Volume 12
Number 42
14 November 2021
Pages 13975–14318

# Chemical Science

rsc.li/chemical-science

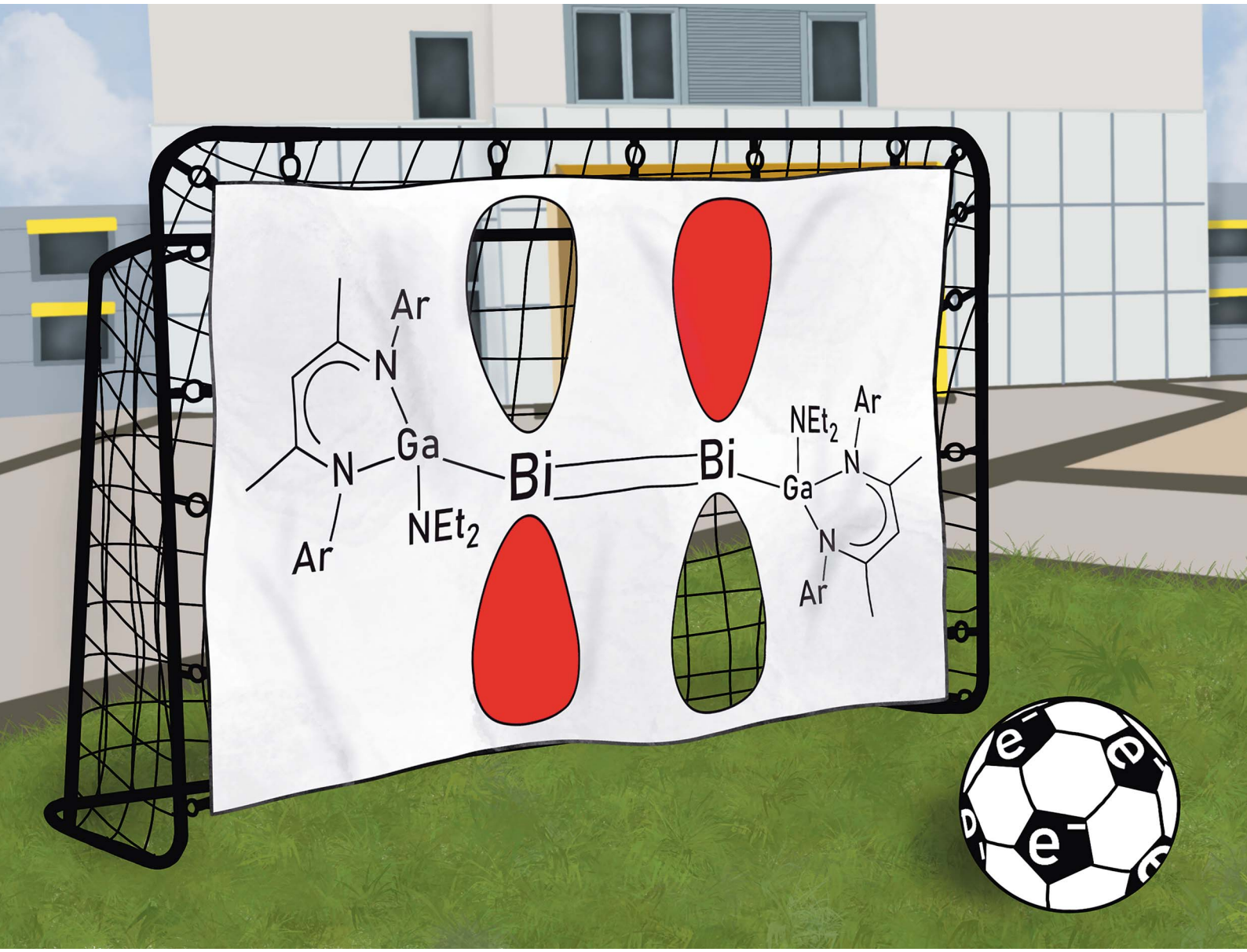


ISSN 2041-6539

ROYAL SOCIETY OF CHEMISTRY

**EDGE ARTICLE**
Stephan Schulz *et al.*
Synthesis, structure and bonding nature of heavy dipnictene radical anions

Chemical Science

ROYAL SOCIETY OF CHEMISTRY

EDGE ARTICLE

View Article Online
View Journal | View Issue



Cite this: *Chem. Sci.*, 2021, **12**, 14024

All publication charges for this article have been paid for by the Royal Society of Chemistry

Received 2nd August 2021
Accepted 28th August 2021

DOI: 10.1039/d1sc04230k

rsc.li/chemical-science



# Synthesis, structure and bonding nature of heavy dipnictene radical anions†

Hanns M. Weinert,[a] Christoph Wölper,[a] Julia Haak,[ab] George E. Cutsail III[ab] and Stephan Schulz *[a]

Cyclic voltammetry (CV) studies of two L(X)Ga-substituted dipnictenes $[L(R_2N)GaE]_2$ (E = Sb, R = Me **1**; E = Bi; R = Et **2**; L = HC[C(Me)NDipp]$_2$; Dipp = 2,6-*i*-$Pr_2C_6H_3$) showed reversible reduction events. Single electron reduction of **1** and **2** with $KC_8$ in DME in the presence of benzo-18-crown-6 (B-18-C-6) gave the corresponding dipnictenyl radical anions (DME)[K(B-18-C-6)][$L(R_2N)GaE]_2$ (E = Sb, R = Me **3**; E = Bi, R = Et **4**). Radical anions **3** and **4** were characterized by EPR, UV-vis and single crystal X-ray diffraction, while quantum chemical calculations gave deeper insight into the nature of the chemical bonding.

## Introduction

Heavy p-block element compounds with π-bonding contribution[1] have received increasing interest after the synthesis of the first stable diphosphene $[Mes^*P]_2$ (Mes* = 2,4,6-*t*-$Bu_3$-$C_6H_2$)[2] and disilene $[Mes_2Si]_2$ (Mes = 2,4,6-$Me_3$-$C_6H_2$)[3] in the 1980s. Heavier dipnictenes $[RE]_2$ (E = As, Sb, Bi) are typically kinetically stabilized by using bulky substituents, *i.e.* carbon-based ligands,[4] amides,[5] boryles,[6] ferrocenyls,[7] and phosphanides.[8] In addition, carbene-coordinated homonuclear π-bonded diatomic p-block elements compounds[9] and L(X)Ga-substituted dipnictenes $[L(X)GaE]_2$ were structurally characterized,[10] and their electronic nature was analysed by quantum chemical calculations.[11] The LUMO of dipnictenes containing σ-bonded ligands is typically represented by low-lying π* orbitals, whereas the level of the molecular orbitals of the π orbitals are somewhat indistinct since their energy levels are close to those of $n_+$ orbital or high lying σ bonds (in phase integration of lone pairs).[12] The HOMO in $[L(X)GaE]_2$ is represented by the Ga–E bond and the LUMO is ligand-centred,[13] while the HOMO and LUMO in carbene-substituted dipnictenes are delocalized *via* the π and π* orbitals of the ligands.[4a]

Dipnictenes react in single-electron transfer reactions to the corresponding radical anions (reduction) or cations (oxidation) as was shown for (carbene-coordinated) diphosphenes,[14] phosphaarsenes,[15] and diarsenes.[16] In contrast, distibene and dibismuthene radical cations have not been reported to date, while radical anions $[(bbt)E]_2^{\bullet-}$ (E = P, Sb, Bi; bbt = 2,6-$[CH(SiMe_3)_2]$-4-$[C(SiMe_3)_3]$-$C_6H_2$) were prepared by reactions of $[(bbt)E]_2$ with Li metal. $[(bbt)Bi]_2^{\bullet-}$ was characterized in solution by UV-vis, whereas EPR measurements failed due to its quick decomposition to EPR silent bbtH.[4b,12b,17] To the best of our knowledge, $[(bbt)Sb]_2^{\bullet-}$ **IV** is the only structurally characterized heavier dipnictene radical anion (Scheme 1).[17]

Heavy main-group element-centred radicals have promising applications in organic synthesis, catalysis, and material sciences.[18,19] Our interest in pnictogen-centred radicals[10f,20] prompted our attention to reduction reactions of L(X)Ga-substituted dipnictenes (L = HC[C(Me)NDipp]$_2$; Dipp = 2,6-*i*-$Pr_2C_6H_3$), and we herein report on the synthesis and structures of two dipnictene radical anions [K(DME)(B-18-C-6)][{$L(R_2N)GaE$}$_2$] (E = Sb, Bi).

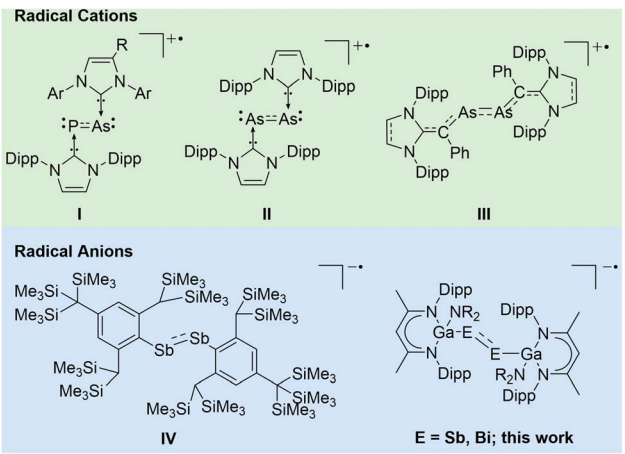


Scheme 1 Structurally characterized heavy dipnictene radical cations and anions (E = As, Sb, Bi).

[a]*Institute for Inorganic Chemistry, Center for Nanointegration Duisburg-Essen (CENIDE), University of Duisburg-Essen, Universitätsstraße 5–7, 45117 Essen, Germany. E-mail: stephan.schulz@uni-due.de*

[b]*Max Planck Institute for Chemical Energy Conversion (CEC), Stiftstraße 34–36, 45470 Mülheim a. d. Ruhr, Germany*

† Electronic supplementary information (ESI) available: Detailed synthetic procedures and analytical data, NMR, IR, EPR, and UV-vis spectra, computational details and cif files. CCDC 2077932 (**3**) and 2080779 (**4**). For ESI and crystallographic data in CIF or other electronic format see DOI: 10.1039/d1sc04230k

## Results and discussion

### Cyclic voltammetry

CV studies of dipnictenes $[L(Me_2N)GaSb]_2$ **1** [10b] and $[L(Et_2N)GaBi]_2$ **2** [10d] were performed in saturated THF solution with $NBu_4PF_6$ as the electrolyte salt at 45 °C (Fig. 1).

**1** and **2** showed reversible reduction events at −1.90 V (**1**) and −2.26 V (**2**) *vs.* the $Fc^{0/+}$ couple with rather low peak-to-peak separation, which only moderately increased with increasing scan rate (Fig. S14 and S15†).[21] Comparable findings were reported for dipnictenes $[bbtE]_2$ (E = Sb −1.74 V, Bi −1.89 V [12b] using 0.09 V Fc *vs.* $Ag/Ag^+$).[22] However, $[bbtE]_2$ showed higher reduction potentials than **1** and **2** (Bi $\Delta E_{1/2}$ = 0.39 V; Sb $\Delta E_{1/2}$ = 0.16 V). Dibismuthene **2** also showed an irreversible oxidation event at $E_{pa}$ = −0.12 V, whereas a second irreversible reduction reaction at −2.90 V was found for distibene **1**, which indicates the reduction of initially formed radical anion to the corresponding dianion. Moreover, a pseudo reversible reduction event at $E_{1/2}$ = −1.2 V ($\Delta E_{pa/c}$ = 0.5 V, $Ag/Ag^+$ or AgCl) was reported for $[L(TfO)GaBi]_2$,[10a] which largely deviates from the potential we obtained for **2**. Even assuming a high difference of 0.4 V to the $Fc^{0/+}$ this is still shifted 0.7 V to lower potential.[23]

### Radical synthesis

Dipnictenes $[L(R_2N)GaE]_2$ (E = Sb, R = Me **1**; E = Bi, R = Et **2**) were reacted with reducing agent, *i.e.* Li, Na, K, alkaline metal naphthalenides and $KC_8$, in ether or toluene solution in the presence or absence of crown ethers and cryptands.

Suspensions of **1** and **2** quickly dissolved upon addition of the reductant with formation of dark green or brown solutions, which showed broad resonances in the $^1H$ NMR spectra (Fig. S10 and S11†), indicating the formation of radical anions.

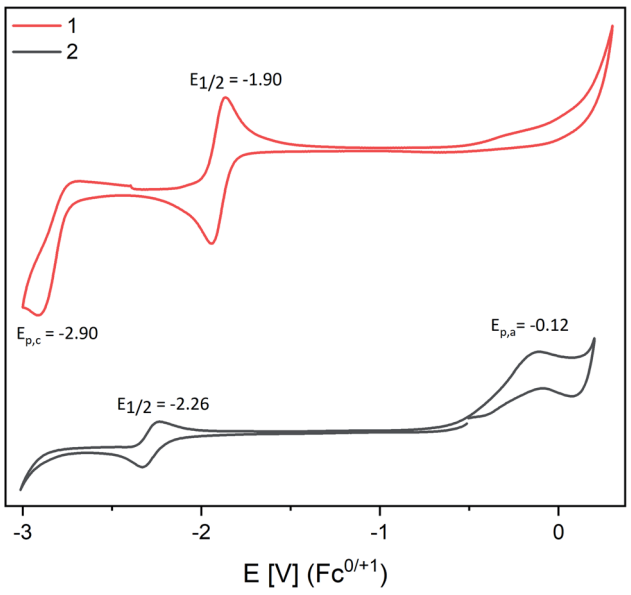


Fig. 1 CV curves of saturated solutions of **1** and **2** in THF with $[n\text{-}Bu_4N][PF_6]$ (100 mM) as electrolyte. Experiments were performed at 45 °C due to the low solubility of **1** and **2**.

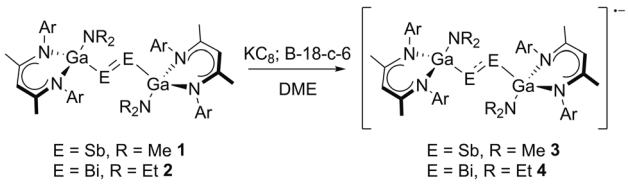


Scheme 2 Synthesis of dipnictene radical anions **3** and **4** by reduction of dipnictenes **1** and **2**; Ar = Dipp.

As-formed radicals typically decomposed to the corresponding dipnictene and metallic pnictogene within a short period of time, but $(DME)[K(B\text{-}18\text{-}C\text{-}6)][L(R_2N)GaE]_2$ (E = Sb, R = Me **3**; E = Bi, R = Et **4**) were finally isolated from reactions of dipnictenes **1** and **2** in DME with $KC_8$ in the presence of B-18-C-6 (Scheme 2) as green (**3**) and brown powders (**4**), respectively.

**3** showed broad resonances in the $^1H$ NMR. The effective magnetic moment $\mu_{eff}$ of 1.85 $\mu_B$ (Evans method, Fig. S1†) agrees with the expected value for an unpaired electron ($\mu_{eff}$ = 1.73 $\mu_B$), confirming the radical character of **3**.[24] Solutions of **3** were fairly stable in solution and in the solid state, whereas **4** was found to decompose in ether or toluene solutions even at low temperature (−35 °C) as well as in isolated crystalline form. Radical anion **4** was therefore only isolated in low yield (28%) by fast precipitation from a concentrated DME solution upon addition of *n*-hexane. The low thermal stability of radical anion **4** prevented it from purification by recrystallization, and all attempts yielded mixtures of the dibismuthene **2**, radical anion **4** and elemental bismuth. The lower effective magnetic moment $\mu_{eff}$ of 1.50 $\mu_B$ as determined by use of the Evans method (Fig. S2†) most likely results from presence of small amounts diamagnetic impurities, *i.e.* dibismuthene **2** which was observed by $^1H$ NMR spectroscopy. No paramagnetic species was detected by use of the Evans method (Fig. S13†) after storing a solution of **4** in THF for 6 h due to complete decomposition. The solution of **4** turned greenish during this time and a large amount of elemental bismuth formed within 24 h. Tokitoh *et al.* reported comparable findings for dibismuthene radical anion $[(bbt)Bi]_2^{\bullet-}$, which was formed as dark brown

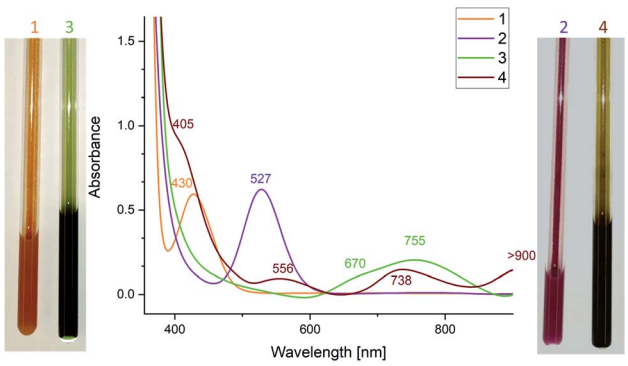


Fig. 2 UV-vis spectra of dipnictenes **1** and **2** in benzene and dipnictene radical anions **3** and **4** in THF solution. To illustrate the colour change, pictures of solutions of 10 mg of **1** and **2** before and after addition of one equivalent of $KC_8$ in NMR tubes are depicted.

solution in the reduction of $[(bbt)Bi]_2$ with metallic lithium,[17] but EPR measurements even from freshly prepared samples failed due to its fast decomposition.

The UV-vis spectrum of $[(bbt)Bi]_2^{\bullet-}$ showed a maximum at 804 nm which was assigned to the π–π* transition. UV-vis spectra of **3** (755 nm) and **4** (556, 738 nm) also showed absorption maxima in the visible region (Fig. 2), which are redshifted compared to neutral dipnictenes **1** (430 nm) and **2** (527 nm), indicating weakened π-bonds. The absorption band of **3** is in between the absorption maxima reported for $[(bbt)Sb]_2^{\bullet-}$ and π–π* transitions calculated for $[MesSb]_2^{\bullet-}$ (Mes = mesityl) radical anions (812, 728 nm).[17]

## Crystallography

Single crystals were obtained from solutions in DME layered with *n*-hexane at −35 °C (**3**) and −30 °C (**4**). **3** and **4** (Fig. 3 and 4) crystallize in the monoclinic space group $P2_1/c$.

The Sb–Sb bond in **3** (2.7359(3) Å) is elongated compared to that in distibene $[L(Me_2N)GaSb]_2$ **1** (2.6477(3) Å), but shorter than Sb–Sb single bonds in distibanes $Sb_2R_4$ (2.77–3.07 Å)[25] and $\{[L(Cl)Ga](Ph)Sb\}_2$ (2.8209(4) Å, Table 1),[26] in agreement with a partially filled π*-orbital in radical anion **3**. The Ga–Sb–Sb bond angle increases from distibene **1** (94.710(8)°) to radical anion **3** (100.41(1)°, 101.05(1)°), whereas neutral radicals $[L(X)Ga]_2Sb$ show slightly larger Ga–Sb–Ga bond angles (Cl: 104.89(1)°, Br: 103.47(5)°, I: 107.31(2)°).[20a,c] The Ga–Sb bond in radical anion **3** is slightly shortened compared to the neutral distibene **1** (2.6200(4) Å) and distibane $\{[L(Cl)Ga](Ph)Sb\}_2$ (2.6255(3) Å), whereas all three Ga–N bonds in **3** are slightly elongated.

The Bi–Bi bond length in the dibismuthene radical anion **4** (2.9266(3) Å) is in between those of the neutral dibismuthene $[L(Et_2N)GaBi]_2$ **2** (2.8132(3) Å) and of dibismuthanes $Bi_2R_4$ (2.98–3.18 Å).[27] The Ga–Bi bond length is slightly shorter than

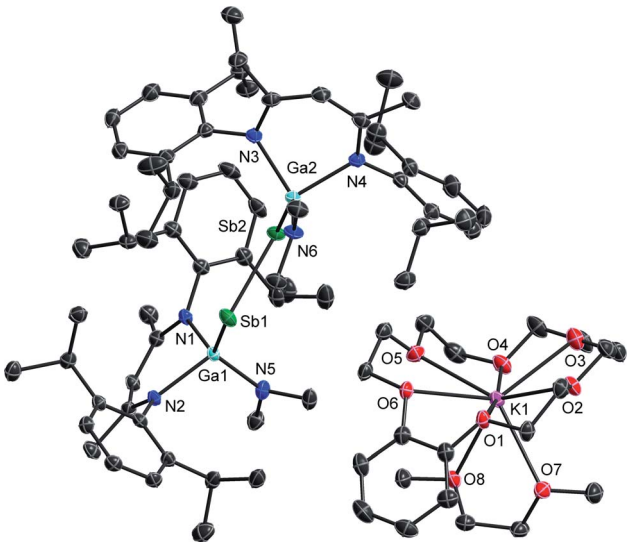


Fig. 3 Molecular structure of **3** in the crystal. H-atoms and solvent molecules are omitted for clarity. Displacement ellipsoids are drawn at the 50% probability level.

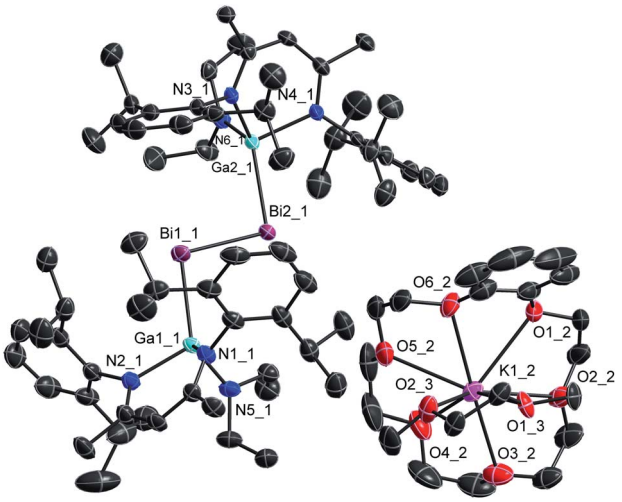


Fig. 4 Molecular structure of **4** in the crystal. H-atoms and minor part of the disorder are omitted for clarity. Displacement ellipsoids are drawn at the 50% probability level.

that of the neutral dibismuthene **2**, whereas all three Ga–N bond lengths in **4** are slightly elongated compared to those in **2** (Table 1). Again, the Ga–Bi–Bi bond angles substantially increased from 95.38(2)° (**2**) to 98.73(1)° and 101.44(1)° for the radical anion **4** as was also observed for distibene radical **3**. The neutral L(X)Ga-substituted radicals $[L(X)Ga]_2Bi$ show slightly larger Ga–Bi–Ga bond angles (Cl: 105.46(1)°, I: 106.68(3)°) again.[10f,20a] These findings contrasts those reported for the only structurally characterized distibene radical anion $[(bbt)Sb]_2^{\bullet-}$ **IV**, which showed a smaller C–Sb–Sb angle compared to the neutral distibene $[(bbt)Sb]_2$.[17] The origin of the increasing Ga–E–E bond angles of **3** and **4** compared to the neutral dipnictenes **1** and **2** is yet unclear. They might result from different intra- and intermolecular interactions including H···H and E···π dispersion interactions as was previously reported,[13a] from interactions of the radical anion with the sterically demanding cation or from packing effects.

## EPR spectroscopy

The formation of the radical anion **3** was confirmed by electron paramagnetic resonance (EPR) spectroscopy. The continuous wave (CW) X-band (~9.43 GHz) EPR spectrum of the THF solution at room temperature exhibits a highly broadened signal, centred at $g_{iso} = 2.16$ (Fig. 5).

The large *g*-shift observed from $g_e$ is the result of a large spin–orbit contribution (SOC) of the unpaired electron, supporting that the radical is metal-centred at the antimony atom(s).[28] The CW X-band EPR spectrum of the frozen solution (Fig. 5) shows a broad signal with broad hyperfine features, due to the coupling of the unpaired electron with two Sb atoms. The frozen solution EPR of **3** may be simulated with a slightly rhombic *g*-tensor, $\boldsymbol{g} = [2.401, 2.051, 2.000]$, that has a $g_{iso}$ value of 2.15, in good agreement with that measured at room temperature. The Sb hyperfine of the simulation, $\mathbf{A}(^{121}Sb) = [120, 200, 560]$ MHz, is approximately axial with a maximum

Table 1 Selected bond lengths [Å] and angles [°] of **1–4**, pnictanyl radicals $R_2E^{\bullet}$ (R = [L(Cl)Ga], E = Sb, Bi) and distibane [R(Ph)Sb]$_2$

| | E–E | Ga–E | Ga–X[a] | Ga–N | Ga–E–Y[c] | N–Ga–N | X–Ga–E[a] |
|---|---|---|---|---|---|---|---|
| **1** (ref. 10b) | 2.6477(3) | 2.6200(4) | 1.856(1) | 1.983(1), 1.989(1) | 94.710(8) | 93.16(5) | 116.37(4) |
| **3** | 2.7359(3) | 2.5826(4), 2.6052(4) | 1.886(2), 1.881(1) | 2.027(2), 2.004(2), 2.038(2), 2.038(2) | 100.41(1), 101.05(1) | 91.36(9), 90.84(9) | 120.25(7), 126.07(7) |
| [R(Ph)Sb]$_2$ (ref. 26) | 2.8209(4) | 2.6255(3) | 2.2208(6) | 1.958(2), 1.953(2) | 102.80(1), 114.33(6)[b] | 95.82(7) | 116.78(2) |
| $R_2Sb^{\bullet}$ (ref. 20a) | | 2.5909(3), 2.5899(4) | 2.2028(7), 2.1623(9) | 1.956(2), 1.959(2), 1.961(2), 1.969(2) | 104.89(1) | 95.78(8), 95.69(8) | 121.46(2), 119.26(3) |
| **2** (ref. 10d) | 2.8132(5) | 2.7061(6) | 1.884(5) | 2.006(4), 2.005(4) | 95.38(2) | 93.4(2) | 114.9(1) |
| **4** | 2.9266(3) | 2.6992(5), 2.6759(5) | 1.890(4), 1.902(3) | 2.057(3), 2.040(3), 2.036(3), 2.025(3) | 101.44(1), 98.73(1) | 91.6(1), 91.8(1) | 128.8(1), 123.6(1) |
| $R_2Bi^{\bullet}$ (ref. 10f) | | 2.6485(3), 2.6619(4) | 2.2084(7), 2.2113(8) | 1.968(2), 1.955(2), 1.955(2), 1.964(2) | 105.46(1) | 95.2(1), 95.7(1) | 123.08(2), 112.92(3) |

[a] X = Cl except for **1**/**3** ($NMe_2$) and **2**/**4** ($NEt_2$). [b] C–Sb–Sb. [c] Y = E for **1–4**, any other Y = Ga.

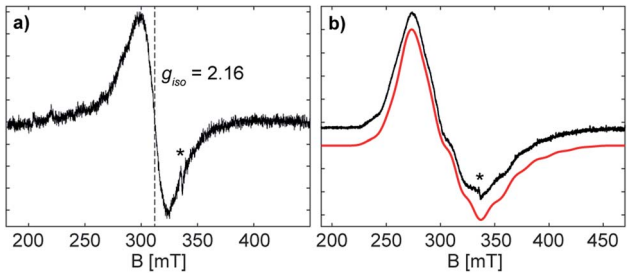


Fig. 5 Continuous-wave EPR spectra of **3** (a) as solution in THF collected at X-band frequency (~9.43 GHz) and (b) as frozen solution (77 K) collected at X-band frequency (~9.45 GHz) in black with simulated spectrum in red. The asterisk indicates a small organic radical impurity. The frozen solution EPR (b) shows a broad signal with broad hyperfine features, due to the coupling of the unpaired electron with two Sb atoms, each of which possess NMR-active nucleotides ($^{121}$Sb 57.21%, $I$ = 5/2; $^{123}$Sb 42.79%, $I$ = 7/2). EPR simulation parameters: $\boldsymbol{g}$ = [2.401, 2.051, 2.000], 2 × A($^{121}$Sb) = [120, 200, 560] MHz, lw (linewidth, peak-to-peak) = 13 mT; spectrometer conditions are described in the Experimental section.

coupling of 560 MHz. The large line broadening observed is possibly due to additional unresolved hyperfine features (*i.e.* the $^{69/71}$Ga nuclei). The maximum Sb coupling of **3** is nearly half of that of the maximum Sb couplings observed in mononuclear Sb radical centres with similar Ga coordinating ligands,[20a,28] and the estimated EPR parameters of **3** correspond well with the reported values for the distibene radical anion $[(bbt)Sb]_2^{\bullet-}$ **IV**.[17] The Sb hyperfine coupling observed for **3** and the agreement with a previously characterized distibene radical both support the assignment of the unpaired electron of **3** as delocalized in a Sb–Sb π* orbital.

The CW X-band EPR spectrum of the frozen solution of **4**, (Fig. S16†), shows a highly broadened signal, that expands over a range from 100 mT to 550 mT. A multiline pattern is observed with approximately equal splitting of 20 mT (~500 MHz), originating from the hyperfine interaction of the unpaired electron with the Bi nuclei ($^{209}$Bi 100%, $I$ = 9/2). This observed splitting is not assignable to any conical hyperfine value. The X-band EPR spectrum of **4** is significantly narrower than the spectrum of the mononuclear analogue $[L(I)Ga]_2Bi^{\bullet}$, whose X-band EPR spectrum expands over 800 mT.[20a] Assuming the same degree of $g$-anisotropy for both, a mono- and a dinuclear bismuth radical, this reduction in width of the EPR spectrum would be primarily due to a decrease in the Bi hyperfine interaction, supporting the delocalization over two metal centres as assigned by the crystal structure of **4**.

The EPR spectrum of **4** at W-band frequency (94.01 GHz) (Fig. S16†) exhibits well separated $g$-values, but lacks resolved hyperfine features, probably due to additional strain at higher frequencies.[29] Two EPR spectral components are observed with $g_1$-values of 3.12 and 2.52 (Fig. S17†), whose origin is currently unknown; EPR measurements of multiple samples of both frozen solution and solid suspensions exhibit both components. Nonetheless, the significant shifts from $g_e$ are in line with increased SOC for heavier elements and supporting of a bismuth-centred radical.[28] Simulations (Fig. S17†) allow for estimates of a maximum Bi hyperfine coupling of 700 MHz. This value is significantly smaller than the minimum coupling of ~2800 MHz resolved by Schwamm *et al.*[30] With respect to the weak Bi–Bi bond in **4**, this radical anion may be prone to decomposition even at low temperatures, making the formation of another Bi radical possible. As discussed earlier, the significantly narrower EPR spectrum of **4** at X-band compared to $[L(I)Ga]_2Bi^{\bullet}$ eliminates the possible formation of a mononuclear Bi radical. In conclusion, the small hyperfine estimates, inferred from both the X- and W-band EPR spectra, is suggestive of a radical species delocalized over two bismuth atoms.

## Quantum chemical calculations

The bonding nature and electronic structure of radical anions **3** and **4** were investigated by quantum chemical calculations at the PBE0 level of theory, and the results were compared to those obtained for neutral dipnictenes **1** and **2** to reveal electronic differences within the $M_2E_2$ unit.[31] Calculated bond lengths within the $M_2E_2$ skeleton (Table 2) are in good agreement with the experimental values ($\Delta r$ = 0.5–6 pm), even though one Ga atom in **4** is tilted out of the $M_2E_2$ plane.[32] The spin density is concentrated within the $E_2$ unit (Fig. 6 and 7), occupying the π*

Table 2 Calculated X–Y bond lengths ($r$, Å) (exp.), X and Y NPA (AIM) atomic charges ($q$, $|e|$), Wiberg bond indices (WBI), occupation numbers (ON, $|e|$) of the $\sigma_{XY}$ bonds according to NBO analysis of [L($Me_2$N)GaSb]$_2$ **1** and [L($Et_2$N)GaBi]$_2$ **2**, (DME)[K(B-18-C-6)][L($Me_2$N)GaSb]$_2$ **3**, and (DME)[K(B-18-C-6)][L($Et_2$N)GaBi]$_2$ **4**

| | X–Y | $r$(X–Y) | $q$(X) | $q$(Y) | WBI | ON[a]a |
|---|---|---|---|---|---|---|
| **1** | Ga1–Sb1 | 2.6040 (2.6200(4)) | 1.36 (1.37) | −0.16 (−0.16) | 0.97 | 1.96 (0.392/0.608) |
| | Ga2–Sb2 | 2.6049 (2.6200(4)) | 1.38 (1.34) | −0.16 (−0.16) | 0.96 | 1.96 (0.390/0.601) |
| | Sb1–Sb2 | 2.6229 (2.6477(3)) | | | 1.82 | σ 1.95(0.502/0.498) |
| | | | | | | π 1.91 (0.501/0.499) |
| | Sb1/2 lone-pair | | | | | 1.94/1.93 |
| **2** | Ga1–Bi1 | 2.6737 (2.7061(6)) | 1.33 (1.33) | −0.10 (−0.11) | 0.98 | 1.96 (0.411/0.589) |
| | Ga2–Bi2 | 2.6737 (2.7061(6)) | 1.33 (1.36) | −0.10 (−0.20) | 0.98 | 1.96 (0.412/0.588) |
| | Bi1–Bi2 | 2.7712 (2.8132(5)) | | | 1.81 | σ 1.94 (0.499/0.501) |
| | | | | | | π 1.90 (0.500/0.500) |
| | Bi1/2 lone-pair | | | | | 1.95/1.95 |

| | X–Y | $r$(X–Y) | $q$(X) | $q$(Y) | WBI | ON($\alpha$) | ON($\beta$)[a] |
|---|---|---|---|---|---|---|---|
| **3** | Ga1–Sb1 | 2.5633 (2.5826(4)) | 1.35 (1.27) | −0.49 (−0.39) | 1.08 | 0.95 (0.376/0.624) | 0.95(0.386/0.614) |
| | Ga2–Sb2 | 2.5595 (2.6052(4)) | 1.37 (1.24) | −0.51 (−0.39) | 1.08 | 0.95 (0.377/0.623) | 0.95 (0.383/0.617) |
| | Sb1–Sb2 | 2.7312 (2.7359(3)) | | | 1.37 | σ 0.97 (0.500/0.500) | σ 0.97 (0.499/0.501) |
| | | | | | | | π 0.93 (0.494/0.506) |
| | Sb1/2 lone-pair | | | | | 0.96/0.92 | 0.96/0.95 |
| **4** | Ga3–Bi1 | 2.6407(2.6992(5)) | 1.34 (1.24) | −0.44 (−0.33) | 1.09 | 0.95 (0.339/0.605) | 0.94 (0.406/0.594) |
| | Ga4–Bi2 | 2.6386 (2.6759(5)) | 1.34 (1.24) | −0.47 (−0.35) | 1.09 | 0.94 (0.391/0.609) | 0.94 (0.400/0.600) |
| | Bi1–Bi2 | 2.8895 (2.9266(3)) | | | 1.35 | σ 0.97 (0.503/0.407) | σ 0.97 (0.501/0.499) |
| | | | | | | | π 0.92 (0.476/0.524) |
| | Bi1/2 lone-pair | | | | | 0.96/0.92 | 0.96/0.95 |

[a] Squared polarization coefficients cX ($|cX|^2$) of the $\sigma_{XY}$ bond NBOs.

orbital. The SOMOs of **3** and **4** are similar to the LUMOs of **1** and **2** in agreement with the observed reversible reduction reactions. The calculated natural (Becke)[33] spin densities show 92% (87%) location at the Sb centres and 3% (5%) at the Ga centres for **3**, as well as 92% (89%)[34] location at the Bi centres and 3% (4%) at the Ga centres for **4**. In contrast, a contribution of 32% and 24% were reported for the $As_2$ unit of divinyldiarsene **III** radical cations, with a higher density at the proximal carbon atoms (30% and 40%).[16a]

Atoms in molecules (AIM), electron localization function (ELF), and natural bond orbital (NBO) analyses were performed to study the bonding situation of **1** to **4** (Table 2, Fig. S19 and Tables S2–S5†).[35] NBO analyses revealed the formation of two-centre-two-electron $\sigma_{E-E}$ and $\pi_{E-E}$ bonds with occupation numbers (ON) of 1.94, 0.93$e$ for **3** and 1.94, 0.92$e$ for **4**, respectively. Compared to neutral dipnictenes (ON 1.95, 1.91$e$ **1**; 1.94, 1.90$e$ **2**) there is less electron density in the π-bonding orbital reflected by the reduced Wiberg bond indices (WBI) [1.82 (**1**) *vs.* 1.37 (**3**) and 1.81 (**2**) *vs.* 1.35 (**4**)].

ELF distribution reveals two disynaptic V(E,E) basins and two monosynaptic V(E) basins, and the occupation shifts towards monosynaptic basins for radical anion ($\bar{N}$[V(Sb)] = 2.7 to 3.7$e$ and $\bar{N}$[V(Sb–Sb)] = 1.4 to 0.9$e$ and $\bar{N}$[V(Bi)] = 2.9 to 4.0$e$ and $\bar{N}$[V(Bi–Bi)] = 1.3 to 0.7$e$). The increase in natural charge from −0.16 (**1**) to −0.50$e$ (**3**) and −0.10 (**2**) to −0.46$e$ (**4**) indicates a localization of the negative charge with in the $E_2$ unit, whereas the natural charge on the Ga centres is not affected. However, the WBI for the Ga–E bond moderately increases from 0.97 (**1**) to 1.08 (**3**) and 0.98 (**2**) to 1.09 (**4**), which clearly reflects the shorter Ga–E bond as observed in the solid state. The number of electrons in the ELF basin remains the same

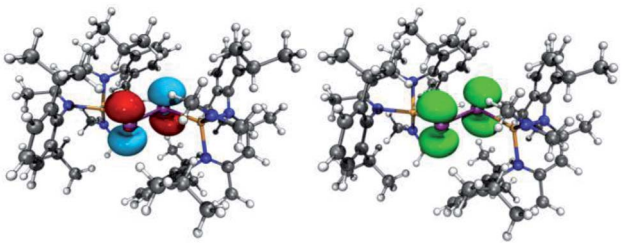

Fig. 6 (left) LUMO of [L($Me_2$N)GaSb]$_2$ **1** (isovalue 0.05). (right) Spin density of (DME)[K(B-18-C-6)][L($Me_2$N)GaSb]$_2$ **3**.

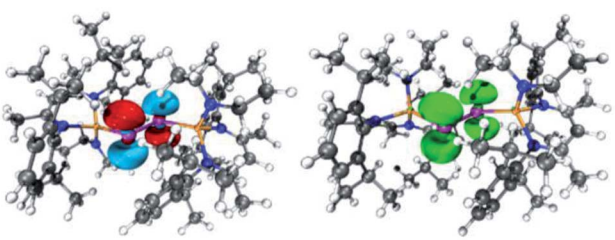

Fig. 7 (left) LUMO of [L($Et_2$N)GaBi]$_2$ **2** (isovalue 0.05). (right) Spin density of (DME)[K(B-18-C-6)][L($Et_2$N)GaBi]$_2$ **4**.

Table 3 Calculated and experimental adsorption maxima [nm] of $\pi \rightarrow \pi^*$ transitions for $[(bbt)E]_2$, $[(bbt)E]_2^{\bullet-}$ (E = Sb, Bi) and **1–4**[17]

| | Calculated[a] | Experimental |
|---|---|---|
| [(bbt)Sb] | 434 | 490 |
| $[(bbt)Sb]_2^{\bullet-}$ | 728 | 812 |
| **1** | 419 | 430 |
| **3** | 723 | 755 |
| [(bbt)Bi] | 470 | 537 |
| $[(bbt)Bi]_2^{\bullet-}$ | 804 | 805 |
| **2** | 465 | 527 |
| **4** | 849 | >900 |

[a] Calculated for a model system with mesitylene instead of bbt.

(V(Ga,Sb) = 2.2*e*, V(Ga,Bi) = 2.2*e*), but the contribution of the electrons of gallium according to ELF/AIM intersection procedure ([V(Ga,Sb)|Ga]) increases from 1.00*e* (**1**,**2**) to 1.15*e* (**3**) and 1.20*e* (**4**).[36] The ON of 1.9*e* and $|V(r_b)|/G(r_b)$ = 2.4 (**3**) 2.2 (**4**) indicate a covalent Ga–Sb and Ga–Bi interaction for **3**. In addition, weak orbital interaction between the $\pi^*_{E-E}$ and the $\sigma^*_{Ga-N}$ orbital were observed (NBO), and elongated Ga–N bonds found in the solid state.

TDDFT calculation of **1–4** were performed and compared to experimental UV-vis spectra (Table S6 and Fig. S20–S23†).[31] The transitions of **1** and **3** agree well with the experimental values and known $\pi \rightarrow \pi^*$ transitions (Table 3). The transitions of the radical anions are redshifted compared to those of the neutral species as was previously reported for the aryl-substituted species $[(bbt)Sb]_2^{\bullet-}$ and $[(bbt)Bi]_2^{\bullet-}$,[4b,12b,17] respectively.

The calculated absorptions of **2** and **4** deviate slightly more from the experimental values than those of **1** and **3**. Moreover, **4** shows a larger redshift than the corresponding bbt substituted radical anion $[(bbt)Bi]_2^{\bullet-}$, indicating a lower lying SOMO of **4**. The gallium-based ligands seem to bind stronger to the bismuth centre compared to the bbt substituents, which also explains the higher thermal stability of **4** in solution when compared to $[(bbt)Bi]_2^{\bullet-}$. These findings might result from a better orbital overlap due to the comparable size of gallium and bismuth as well as the higher electropositive nature of gallium compared to carbon, which supports the stabilization of the negative charge.

## Conclusions

$L(R_2N)Ga$-substituted dipnictenes $[L(R_2N)GaE]_2$ (E = Sb, R = Me **1**; E = Bi, R = Et **2**) showed reversible reduction events in cyclic voltammetry studies. Reduction of distibene **1** and dibismuthene **2** with $KC_8$ in the presence of B-18-C-6 yielded rare dipnictene radical anions (DME)[K(B-18-C-6)][$L(R_2N)GaE]_2$ (E = Sb, R = Me **3**; E = Bi, R = Et **4**), which were characterized by single-crystal X-ray diffraction. **4** represents the first structurally characterized dibismuthene radical anion, and the radical nature of **3** and **4** was confirmed by EPR spectroscopy. Quantum chemical calculations revealed the different bonding nature in compounds **1–4** and are in accordance with the formation of pnictogen-centred radicals **3** and **4** due to a high localization of spin density and charge within the central $E_2$ unit. The elongated E–E and shorter Ga–E bond lengths of radicals **3** and **4** compared to the neutral dipnictenes **1** and **2** result from the population of the $\pi^*_{E-E}$ orbital with one electron, leading to a formal bond order of 1.5.

The capability of the L(X)Ga substituent for the stabilization of unusual main group metal compounds most likely results from its rather electropositive nature, which reduces orbital energies as was recently reported for the silylene $[L(Br)Ga]_2Si$, which reacted with carbon monoxide with formation of the first room temperature-stable silylene–carbonyl complex.[37] We assume that the introduction of L(X)Ga substituents to the $E_2$ unit of the dipnictenes **1** and **2** lowers the SOMO energies of the radical anions compared to aryl-substituted species, hence allowing its population with one electron in radical anions **3** and **4**. In addition, the Ga–E bonds in the radical anions **3** and **4** are slightly stronger compared to those in the neural dipnictenes **1** and **2** (WBI increase of 0.11, Table 2), thus reducing the tendency of radical anions to undergo bond homolysis reaction with formation of elemental pnictogenes.

## Experimental

### General procedures

All manipulations were carried out using standard Schlenk and glove-box techniques under argon, which was dried by passing through pre-heated $Cu_2O$ pellets and molecular sieves columns. *n*-Hexane and toluene were dried with a MBraun Solvent Purification System, benzene, THF, DME as well as deuterated THF and benzene were distilled from Na/K alloy. All solvents were degassed and stored over activated molecular sieves (4 Å). $[L(Me_2N)GaSb]_2$[10b] and $[L(Et_2N)GaBi]_2$[10d] were prepared according to literature methods. $^1$H (300 MHz) spectra were recorded using a Bruker Avance DPX-300 spectrometer and referenced to internal $C_6D_5H$ ($^1$H: $\delta$ = 7.16 or THF-$d_8$ ($^1$H: $\delta$ = 1.72). Solution-state magnetic susceptibilities $\chi_M$ and effective magnetic moments $\mu_{eff}$ were determined by $^1$H NMR spectroscopy using Evans method[24] with pure solvent as internal reference and neglecting diamagnetic contributions.[38] IR spectra were recorded in a glovebox using a Bruker ALPHAT FT-IR spectrometer equipped with a single reflection ATR sampling module. Cyclic voltammetry studies were performed in a glovebox using a Metrohm Autolab PGSTAT 204 potentiostat with a three electrodes setup consisting of a Pt disc ($d$ = 1 mm) working electrode, Pt wire counter electrode, and Ag wire pseudo-reference electrode, and ferrocene as internal standard. Positive feedback compensation was utilized to reduce solvent resistance effects. UV-vis-spectra were recorded on a Shimadzu UV-2600i spectrophotometer in closed glass cuvette (10 mm) under an argon atmosphere.

The samples of **3** in THF for the EPR measurements were prepared in a glovebox in either 50 μL capillaries (Hirschmann), sealed with Critoseal, or frozen in custom 4 mm (OD) quartz EPR tubes. Continuous-wave (CW) X-band EPR spectra at room temperature (~9.43 GHz) and at 77 K (~9.45 GHz) were collected with a Bruker MS 5000 spectrometer. The spectra were obtained with 100 kHz field modulation frequency, 8 G

modulation amplitude, 30 mW microwave power and a scan time of 360 s. An effective time constant of 0.05 s was applied digitally to the ~60 *k* point spectrum. For the spectra at room temperature and at 77 K, six and three scans were acquired, respectively. EPR samples of **4** were freshly prepared in DME and then filled in custom 2.8 mm (OD, X-band) and 0.9 mm (OD, W-band) quartz EPR tubes and frozen immediately. CW X-band EPR spectra of **4** were collected at ~6 K on a Bruker Elexsys E500 equipped with an Oxford helium flow cryostat and temperature controller. The X-band spectra of **4** were collected with the following parameters: modulation amplitude: 6 G; modulation frequency: 100 kHz; time constant: 81.92 ms; scan time: 336 s; single scan. W-band pulsed EPR measurements of **4** were collected on a Bruker Elexsys E680 spectrometer at ~7 K equipped with a closed cycle helium cryostat system. The spectra were collected with a two-pulse 'Hahn' sequence ($\pi/2$–$\tau$–$\pi$–$\tau$–echo) with the following parameters: $\pi/2 = 20$ ns; $\tau = 400$ ns; repetition rate = 60 μs; effective shots per point: 11 060; effective number of points: 4000; 2 scans. The magnet was swept both up and down at the same sweep rate and the offsets averaged to account for sweep delays. The EPR data was processed and analysed in Matlab R2019b and simulated using the EasySpin package (v. 6.0.0-dev.30).[39]

### Synthesis of (DME)[K(B-18-C-6)][L(Me$_2$N)GaSb]$_2$ (3)

[L(Me$_2$N)GaSb]$_2$ **1** (110 mg, 84 μmol), $KC_8$ (11.4 mg, 84 μmol) and B-18-C-6 (26.3 mg, 84 μmol) were suspended in 4 ml of DME at 0 °C and the suspension was stirred for 1 h, upon which a dark green solution formed, which was concentrated to 1 ml and filtered. The filtrate was further concentrated to almost dryness and layered with *n*-hexane and stored at ambient temperature, yielding a green crystalline powder which was isolated by filtration. Single crystals were obtained upon storage of a solution of **3** in DME that was layered with *n*-hexane at −35 °C.

Yield: 144 mg (80 μmol, 95%). Anal. calcd for $C_{82}H_{128}Ga_2KN_6O_8Sb_2$: C, 56.34; H, 7.38; N, 4.81. Found: C, 56.0; H, 7.49, N 4.61% ATR-IR: $\nu$ 3058, 2955, 2859, 2740, 1438, 1399, 1317, 1248, 1175, 1109, 1092, 969, 793, 741, 523, 439 cm$^{-1}$. $^1$H NMR (300 MHz THF-d$_8$, 25 °C): $\mu_{eff} = 1.85\ \mu_B$. No coalescence was observed at −100 °C.

### Synthesis of (DME)[K(B-18-C-6)][L(Et$_2$N)GaBi]$_2$ (4)

[L(Et$_2$N)GaBi]$_2$ **2** (80 mg, 52 μmol), $KC_8$ (7.0 mg, 52 μmol) and B-18-C-6 (16.3 mg, 52 μmol) were suspended in 0.3 ml of DME in a centrifuge vial and shaken for 5 minutes. Solids were separated by centrifugation and the resulting dark brown solution was mixed with 10 ml of *n*-hexane and stored at −30 °C for 30 min. The resulting cloudy supernatant was removed, and **4** was isolated as a dark brown crystalline solid, which washed with *n*-hexane twice. Storage of a freshly prepared solution of **4** in DME that was layered with *n*-hexane at −30 °C yielded few crystals suitable for SC-XRD.

Yield: 28 mg (14 μmol, 28%). Anal. calcd for $C_{86}H_{136}Bi_2Ga_2KN_6O_8$ + one *n*-hexane molecule from unit cell: C, 53.52; H, 7.32; N, 4.07. Found: C, 53.5; H, 7.10, N 4.30%. ATR-IR: $\nu$ 3048, 2946, 2911, 2851, 1501, 1447, 1433, 1390, 1350, 1311, 1245, 1105, 1085, 1051, 950, 932, 789, 753, 736 cm$^{-1}$. $^1$H NMR (300 MHz, THF-d$_8$, 25 °C): $\mu_{eff} = 1.50\ \mu_B$.

## Data availability

All additional data is part of the ESI file.†

## Author contributions

M. W. performed the experiments including quantum chemical calculations, C. W. the single crystal X-ray diffraction and J. H. the EPR measurements. The work was supervised by G. C. and St. S. The manuscript was written through contributions of all authors. All authors have given approval to the final version of the manuscript.

## Conflicts of interest

There are no conflicts to declare.

## Acknowledgements

We are thankful to the Max-Planck-Gesellschaft (GEC) and the Deutsche Forschungsgemeinschaft DFG (St. S., SCHU 1069/23-1) for generous financial support.

## Notes and references

1 (*a*) R. C. Fischer and P. P. Power, *Chem. Rev.*, 2010, **110**, 3877–3923; (*b*) S. Yadav, S. Saha and S. S. Sen, *ChemCatChem*, 2016, **8**, 486–501; (*c*) S. Schulz, *Chem.–Eur. J.*, 2010, **16**, 6416–6428.
2 M. Yoshifuji, I. Shima, N. Inamoto, K. Hirotsu and T. Higuchi, *J. Am. Chem. Soc.*, 1981, **103**, 4587–4589.
3 R. West, M. J. Fink and J. Michl, *Science*, 1981, **214**, 1343–1344.
4 (*a*) M. K. Sharma, S. Blomeyer, B. Neumann, H. G. Stammler and R. S. Ghadwal, *Chem.–Eur. J.*, 2019, **25**, 8249–8253; (*b*) P. K. Majhi, H. Ikeda, T. Sasamori, H. Tsurugi, K. Mashima and N. Tokitoh, *Organometallics*, 2017, **36**, 1224–1226; (*c*) T. Sasamori and N. Tokitoh, *Dalton Trans.*, 2008, 1395–1408; (*d*) T. Sasamori, Y. Arai, N. Takeda, R. Okazaki, Y. Furukawa, M. Kimura, S. Nagase and N. Tokitoh, *Bull. Chem. Soc. Jpn.*, 2002, **75**, 661–675; (*e*) B. Twamley, C. D. Sofield, M. M. Olmstead and P. P. Power, *J. Am. Chem. Soc.*, 1999, **121**, 3357–3367; (*f*) N. Tokitoh, Y. Arai, T. Sasamori, R. Okazaki, S. Nagase, H. Uekusa and Y. Ohashi, *J. Am. Chem. Soc.*, 1998, **120**, 433–434; (*g*) N. Tokitoh, Y. Arai, R. Okazaki and S. Nagase, *Science*, 1997, **277**, 78–80.
5 R. Schwamm and M. P. Coles, *Chem.–Eur. J.*, 2019, **25**, 14183–14191.
6 D. Dange, A. Davey, J. A. B. Abdalla, S. Aldridge and C. Jones, *Chem. Commun.*, 2015, **51**, 7128–7131.
7 M. Sakagami, T. Sasamori, H. Sakai, Y. Furukawa and N. Tokitoh, *Chem.–Asian J.*, 2013, **8**, 690–693.

8 C. von Hänisch and D. Nikolova, *Eur. J. Inorg. Chem.*, 2006, 4770–4773.
9 (*a*) L. P. Ho and M. Tamm, *Dalton Trans.*, 2021, **50**, 1202–1205; (*b*) Y. Wang and G. H. Robinson, *Inorg. Chem.*, 2014, **53**, 11815–11832.
10 (*a*) G. Prabusankar, C. Gemel, P. Parameswaran, C. Flener, G. Frenking and R. A. Fischer, *Angew. Chem., Int. Ed.*, 2009, **48**, 5526–5529; (*b*) L. Tuscher, C. Ganesamoorthy, D. Bläser, C. Wölper and S. Schulz, *Angew. Chem., Int. Ed.*, 2015, **54**, 10657–10661; (*c*) L. Tuscher, C. Helling, C. Ganesamoorthy, J. Krüger, C. Wölper, W. Frank, A. S. Nizovtsev and S. Schulz, *Chem.–Eur. J.*, 2017, **23**, 12297–12304; (*d*) L. Tuscher, C. Helling, C. Wölper, W. Frank, A. S. Nizovtsev and S. Schulz, *Chem.–Eur. J.*, 2018, **24**, 3241–3250; (*e*) J. Schoening, L. John, C. Wölper and S. Schulz, *Dalton Trans.*, 2019, **48**, 17729–17734; (*f*) J. Krüger, C. Wölper and S. Schulz, *Inorg. Chem.*, 2020, **59**, 11142–11151.
11 L. Zhao, S. Pan, N. Holzmann, P. Schwerdtfeger and G. Frenking, *Chem. Rev.*, 2019, **119**, 8781–8845.
12 (*a*) P. Vilarrubias, *Mol. Phys.*, 2017, **115**, 2597–2604; (*b*) T. Sasamori, E. Mieda, N. Nagahora, N. Takeda, N. Takagi, S. Nagase and N. Tokitoh, *Chem. Lett.*, 2005, **34**, 166–167.
13 (*a*) L. Song, J. Schoening, C. Wölper, S. Schulz and P. R. Schreiner, *Organometallics*, 2019, **38**, 1640–1647; (*b*) J. Krüger, J. Schoening, C. Ganesamoorthy, L. John, C. Wölper and S. Schulz, *Z. Anorg. Allg. Chem.*, 2018, **644**, 1028–1033.
14 (*a*) K. Schwedtmann, M. H. Holthausen, C. H. Sala, F. Hennersdorf, R. Fröhlich and J. J. Weigand, *Chem. Commun.*, 2016, **52**, 1409–1412; (*b*) A. Doddi, D. Bockfeld, M.-K. Zaretzke, C. Kleeberg, T. Bannenberg and M. Tamm, *Dalton Trans.*, 2017, **46**, 15859–15864; (*c*) A. Beil, R. J. Gilliard and H. Grützmacher, *Dalton Trans.*, 2016, **45**, 2044–2052; (*d*) S.-S. Asami, S. Ishida, T. Iwamoto, K. Suzuki and M. Yamashita, *Angew. Chem., Int. Ed.*, 2017, **56**, 1658–1662; (*e*) O. Back, B. Donnadieu, P. Parameswaran, G. Frenking and G. Bertrand, *Nat. Chem.*, 2010, **2**, 369–373; (*f*) M. K. Sharma, D. Rottschäfer, S. Blomeyer, B. Neumann, H.-G. Stammler, M. van Gastel, A. Hinz and R. S. Ghadwal, *Chem. Commun.*, 2019, **55**, 10408–10411; (*g*) O. Back, M. A. Celik, G. Frenking, M. Melaimi, B. Donnadieu and G. Bertrand, *J. Am. Chem. Soc.*, 2010, **132**, 10262–10263; (*h*) R. Kinjo, B. Donnadieu and G. Bertrand, *Angew. Chem., Int. Ed.*, 2010, **49**, 5930–5933; (*i*) X. Pan, Y. Su, X. Chen, Y. Zhao, Y. Li, J. Zuo and X. Wang, *J. Am. Chem. Soc.*, 2013, **135**, 5561–5564.
15 (*a*) A. Doddi, D. Bockfeld, M.-K. Zaretzke, T. Bannenberg and M. Tamm, *Chem.–Eur. J.*, 2019, **25**, 13119–13123; (*b*) K. Tsuji, Y. Fujii, S. Sasaki and M. Yoshifuji, *Chem. Lett.*, 1997, **9**, 855–856.
16 (*a*) M. K. Sharma, S. Blomeyer, B. Neumann, H.-G. Stammler, M. van Gastel, A. Hinz and R. S. Ghadwal, *Angew. Chem., Int. Ed.*, 2019, **58**, 17599–17603; (*b*) M. Y. Abraham, Y. Wang, Y. R. Xie, J. Gilliard, P. Wei, B. J. Vaccaro, M. K. Johnson, H. F. Schaefer, P. V. R. Schleyer and G. H. Robinson, *J. Am. Chem. Soc.*, 2013, **135**, 2486–2488.
17 T. Sasamori, E. Mieda, N. Nagahora, K. Sato, D. Shiomi, T. Takui, Y. Hosoi, Y. Furukawa, N. Takagi, S. Nagase and N. Tokitoh, *J. Am. Chem. Soc.*, 2006, **128**, 12582–12588.
18 C. Helling and S. Schulz, *Eur. J. Inorg. Chem.*, 2020, 3209–3221.
19 (*a*) G. Tan and X. Wang, *Chin. J. Chem.*, 2018, **36**, 573–586; (*b*) S. Kundu, S. Sinhababu, V. Chandrasekhar and H. W. Roesky, *Chem. Sci.*, 2019, **10**, 4727–4741; (*c*) M. Abe, *Chem. Rev.*, 2013, **113**, 7011–7088; (*d*) C. Lichtenberg, *Chem.–Eur. J.*, 2020, **26**, 9674–9687.
20 (*a*) C. Ganesamoorthy, C. Helling, C. Wölper, W. Frank, E. Bill, G. E. Cutsail III and S. Schulz, *Nat. Commun.*, 2018, **9**, 87; (*b*) C. Helling, C. Wölper, Y. Schulte, G. E Cutsail III. and S. Schulz, *Inorg. Chem.*, 2019, **58**, 10323–10332; (*c*) C. Helling, C. Wölper, G. E. Cutsail III, G. Haberhauer and S. Schulz, *Chem.–Eur. J.*, 2020, **26**, 13390–13399; (*d*) C. Helling, G. E. Cutsail III, H. Weinert, C. Wölper and S. Schulz, *Angew. Chem., Int. Ed.*, 2020, **59**, 7561–7568.
21 P. Zanello, *Inorganic Electrochemistry: Theory, Practice and Application*, Royal Society of Chemistry, Cambridge, 2003.
22 G. Inzelt, A. Lewenstam and F. Scholz, *Handbook of Reference Electrodes*, Springer, Berlin, Heidelberg, 2013.
23 (*a*) V. V. Pavlishchuk and A. W. Addison, *Inorg. Chim. Acta*, 2000, **298**, 97–102; (*b*) J. R. Aranzaes, M.-C. Daniel and D. Astruc, *Can. J. Chem.*, 2006, **84**, 288–299.
24 D. F. Evans, *J. Chem. Soc.*, 1959, 2003–2005.
25 Cambridge Structural Database, version 5.42, see also: F. H. Allen, *Acta Crystallogr., Sect. B: Struct. Sci.*, 2002, **58**, 380–388, 55 hits containing an Sb–Sb bond classified as a single were found of the type $R_2Sb–SbR_2$ (R defined as non-antimony, c.n. (Sb) = 3). The Sb–Sb bond lengths range from 2.77–3.07 Å (mean of 2.86(5) Å excluding a single highly ring strain structure 2.64 Å).
26 C. Helling, C. Wölper and S. Schulz, *Eur. J. Inorg. Chem.*, 2020, 4225–4235.
27 Cambridge Structural Database, version 5.42, see also: F. H. Allen, *Acta Crystallogr., Sect. B: Struct. Sci.*, 2002, **58**, 380–388, 17 unique hits containing an Bi–Bi bond classified as a single were found of the type $R_2Bi–BiR_2$ (R defined as non-bismuth, c.n. (Bi) = 3). The Bi–Bi bond lengths ranging from 2.98–3.18 Å with a mean of 3.03(4) Å.
28 G. E. Cutsail III, *Dalton Trans.*, 2020, **49**, 12128–12135.
29 W. Hagen, *Coord. Chem. Rev.*, 1999, **190–192**, 209–229.
30 R. Schwamm, J. Harmer, M. Lein, C. Fitchett, S. Granville and M. Coles, *Angew. Chem., Int. Ed.*, 2015, **54**, 10630–10633.
31 The ORCA quantum chemistry package was used and details regarding the quantum chemical calculations are given in the ESI† (*a*) F. Neese, *Wiley Interdiscip. Rev.: Comput. Mol. Sci.*, 2018, **8**, 1–6; (*b*) F. Neese, *Wiley Interdiscip. Rev. Comput. Mol. Sci.*, 2012, **2**, 73–78.
32 In all cases the geometry optimization was started from the geometry obtained by SC-XRD. In case of the dipnictenes radical anion the presence of counter ion disturbs the symmetry, with a different conformation of LX(Ga), as is reflected by the difference of the N-Ga-E-E torsion angle (Sb: 83.3(9) and 20.8(1) Bi: −23.2(1) and −89.6(1)). As no symmetry and other constraints were invoked the

minimum on the energy surface exhibited an asymmetry as well and shift the Ga centre to reduce the repulsion of the ligand. This is only reflected in a small difference of spin density and charge of the Bi centres.

33 A. D. Becke, *J. Chem. Phys.*, 1998, **88**, 2547–2553.

34 Spin density: Bi1 49%, Bi2 43%. Natural charge: Bi1 $-0.44e^{-}$, Bi2 $-0.47e^{-}$.

35 (*a*) C. Kalaiarasi, M. S. Pavan and v. P. Kumaradhas, *Acta Crystallogr., Sect. B: Struct. Sci., Cryst. Eng. Mater.*, 2016, **72**, 775–786; (*b*) P. Kumar, V. Shayam, V. Raghavendra and V. Subramanian, *J. Chem. Sci.*, 2016, **128**, 1527–1536; (*c*) R. F. W. Bader, *Chem. Rev.*, 1991, **91**, 893–928; (*d*) B. Silvi and A. Savin, *Nature*, 1994, **371**, 683–686; (*e*) A. D. Becke and K. E. Edgecombe, *J. Chem. Phys.*, 1990, **92**, 5397–5403; (*f*) L. U. Tian and C. Fei-Wu, *Acta Phys.-Chim. Sin.*, 2011, **27**, 2786–2792.

36 S. Raub and G. Jansen, *Theor. Chem. Acc.*, 2001, **106**, 223–232.

37 C. Ganesamoorthy, J. Schoening, C. Wölper, L. Song, P. R. Schreiner and S. Schulz, *Nat. Chem.*, 2020, **12**, 608–614.

38 G. J. P. Britovsek, V. C. Gibson, S. K. Spitzmesser, K. P. Tellmann, A. J. P. White and D. J. Williams, *Dalton Trans.*, 2002, 1159–1171.

39 S. Stoll and A. Schweiger, *J. Magn. Reson.*, 2006, **178**, 42–55.